RSC Advances

ROYAL SOCIETY OF CHEMISTRY

www.rsc.org/advances

Influence of bimodal pore structure on the CO hydrogenation activity and selectivity of cobalt catalysts

Jungang Wang[a], Hansheng Li[a,b], Debao Li[a], Johan P. den Breejen[c], Bo Hou[*a]

[a] *State Key Laboratory of Coal Conversion ,Institute of Coal Chemistry Chinese Academy of Sciences, Taiyuan, China*

[b] *University of Chinese Academy of Sciences*

Beijing 100049 (P.R. China)

[c] *Shell Global Solutions International B.V., Amsterdam, Netherlands*

(*) corresponding author: Bo Hou, E-mail:houbo@sxicc.ac.cn

Abstract: A series of Co-based catalysts supported on different silica-based bimodal mesoporous materials for Fischer-Tropsch synthesis (FTs) were prepared by the incipient wetness impregnation (IWI) method. The results showed that Co-based catalysts presented a bimodal mesoporous structure. Catalysis and characterization results showed that the bimodal structure strongly influenced the dispersion of cobalt species and the F-T catalytic performance. Moreover, the F-T synthesis results showed that the catalysts with a bimodal pore size distribution of 2.5 and 8 nm or 2.5 and 11 nm had a lower methane selectivity than those with larger pores. The catalyst with a 2.5 and 22 nm pore size distribution showed the highest activity and the highest selectivity to C_{5-11}.

Keywords: Fischer-Tropsch synthesis; Cobalt; bimodal mesoporous

1 Introduction

Recently, the Fischer-Tropsch synthesis (FTs) has received more attentions than ever since it is considered as an effective process to produce wide-range liquid hydrocarbon fuels and high value-added chemicals from relatively abundant resources, such as natural gas, coal and biomass, via synthetic gas[1, 2, 3]. The efficiency of F-T synthesis can be improved by the design of a catalyst with high hydrocarbon selectivity and low methane selectivity.

It has been reported that the FTs activity and selectivity of cobalt based catalyst are affected by a series of factors, such as its surface properties, pore size, active component dispersion and reducibility, of which the pore structure has a significant impact. The studies of different pore

distribution showed that larger cobalt particles, located in the wider pore, were much more active in F-T synthesis with lower methane selectivity than smaller cobalt particles confined in narrower pores [4]. A support with small pore size usually shows high CO conversion but low heavy hydrocarbon selectivity, due to diffusion limitation [5, 6]. Meanwhile, the support with large pore diameter mostly contains small surface area, resulting in low Co surface areas and hence low CO conversion levels. In contrast, bimodal mesoporous materials possibly combine the merit of two kind of pore size distributions. Apart from the cluster size, dispersion of active species, reducibility and the nature of support, the reactivity of cobalt catalysts during F-T synthesis also depends on the pore size and its bimodal distribution[7].

A support with a distinct bimodal pore structure shows advantages in gas-solid catalysis reaction because the large pores may provide pathways for rapid molecular transportation and small pores may provide a large surface area contributing to high diffusion efficiency and dispersion of supported metal simultaneously. As for supported cobalt catalyst, the bimodal pore structure which contains large pores and small pores, not only are beneficial for the mass-transfer of heavy hydrocarbon[8, 9], but also contributes to a higher dispersion of supported cobalt crystallites by the small pores, which enlarges the surface area of the catalyst. Furthermore, it is able to diminish the diffusion resistance by its large pores. The bimodal catalysts show higher activity and lower methane selectivity than single pore ones, which may contribute to the spatial promoted action of bimodal pore structure[10, 11]. However, the effects of different bimodal mesoporous structure on Fischer Tropsch reaction are less studied.

In this work, a series of bimodal mesoporous supports were prepared by sol-gel method. Supported bimodal Co-based catalysts with different bimodal mesoporous size distribution were prepared by IWI method, and were appplied for F-T synthesis. We aim to investigate and disclose the physicochemical properties and catalytic performances of bimodal mesoporous Co-based catalyst in F-T synthesis.

2 Experimental

2.1 Synthesis of bimodal mesoporous supports and catalysts

Cetytrimethyl Ammonium Bromide (CTAB) was purchased from Tianjin Guangfu Fine Chemical Research Institute. Other chemicals were purchased from Shanghai Chemical Company. All chemicals were of analytical grade and used without any further purification.

The bimodal mesoporous supports were prepared using CTAB as surfactant and sodium silicate (Na_2SiO_3) as silicon source. The detailed prepared method of Co-based catalysts with bimodal porous structure followed the procedure reported previously [12,13]. In a typical synthesis, 19.6 g CTAB and quantitative 23 g Na_2SiO_3 were dissolved in 350 ml distilled water at 80 ^oC. After stirred for 30 min, certain proportion ethyl acetate was added dropwise. Then the suspension was stilled for 5 h, aged at 90 ^oC for 48 h. The suspension was filtrated, dried in an oven at 60 ^oC for 12 h, and finally the sample was calcined at the rate of 5 ^oC /min to 550 ^oC and hold for 6 h. The obtained sample denoted as DM-1. The preparation procedure of DM-2, DM-3, DM-4 and DM-5 were similar with that of DM-1, and the corresponding amount of Na_2SiO_3 was 40 g, 52 g, 65 g and 81 g, respectively.

The preparation of catalyst was performed by incipient wetness impregnation (IWI) method. At the beginning, the as-synthesized supports were added into the precomputed ethanol solution containing cobalt nitrate hexahydrate, which was identical to the nominal loading of 15 wt% cobalt (as metal Co). Then, the mixed solutions were stilled for 24 h at room temperature. Finally, the samples were dried at 100 °C for 12 h and then calcined at 400 °C for 6 h with a ramp of 2 °C min^{-1} under the air atmosphere. The obtained different bimodal porous distribution Co-based catalysts corresponding to above supports were denoted as Co/DM-1, Co/DM-2, Co/DM-3, Co/DM-4 and Co/DM-5, respectively.

2.2 Characterization techniques

2.2.1 BET measurements

N_2 adsorption–desorption experiment was conducted at -196 °C with a ASAP-2000 Micromeritics instrument. Nitrogen isotherms were obtained in both adsorption and desorption modes. The surface areas of supports and catalysts were determined by the BET method. The total pore volume (TPV) was calculated from the amount of vapor adsorbed at a relative pressure (P/Po) close to unity, where P and Po were the measured and equilibrium pressures, respectively. Pore

size distribution curves were established from the desorption branches of the isotherm using the BJH model. Before the analysis, the samples were outgassed at 120 ^{o}C for 12 h.

2.2.2 XRD

XRD patterns were recorded at room temperature by Rigaku D/max-RA instrument using Cu-K radiation. The spectra were scanned at a rate of 2 degree/min in the range $2\theta=20 \sim 80^{o}$. The cobalt particle sizes were calculated by using the full width at half maximum (FWHM) value with the help of Scherrer's equation using the most intense reflexion at $2\theta=36.9^{o}$. The crystallite phase was estimated by the data of JCPDS.

The Co_3O_4 particle sizes in the calcined samples were then converted to the corresponding cobalt metal diameters in reduced catalysts by considering the relative molar volumes of Co^0 and Co_3O_4 using the equation: $d(Co^0) = 0.75 \times d(Co_3O_4)$. Then, the Co^0 metal dispersions can be calculated from the mean Co^0 particle sizes assuming a spherical geometry of the metal particles with uniform site density of 14.6 atoms/nm^2 as described in ref. [14] using $D=96/d(Co^0)$, where D is the percentage dispersion and $d(Co^0)$ is the mean particle size of Co^0 in nm.

2.2.3 Scanning electron microscopy

The morphology of the catalysts was determined by using a Hitachi-S-4800 scanning electron microscope (SEM, Hitachi High-Technologies CO., Ltd.) operating at 2.0 ~10.0 kV.

2.2.4 Transmission electron microscopy

Transmission electron microscopy characterization of the samples was carried out by using a FEI Tecnai G2 instrument. The samples were crushed in an agate mortar, dispersed in ethanol and dropped on copper grids.

2.2.5 Temperature programmed reduction

The reduction behavior and the interaction between active phase and support of each catalyst were examined by using temperature programmed reduction technique. The TPR experiments were carried out with a Zeton Altamira AMI-200 unit. 50 mg samples were placed in a quartz tubular reactor, fitted with a thermocouple for continuous temperature measurement. The reactor was heated with a furnace designed and built to stabilize the temperature gradient and minimize

the temperature error. Prior to the hydrogen temperature programmed reduction measurement, the calcined catalysts were flushed with high purity argon at 150 ^{o}C for 1 h, and cooled down to 50 ^{o}C. Then 10% H_2/Ar was switched on and the temperature was raised at a rate of 10 ^{o}C min^{-1} from 50 to 900 ^{o}C (hold 30 min). The gas flow rate through the reactor was controlled by three Brooks mass flow controllers and was 30 cm^3 min^{-1}. The H_2 consumption (TCD signal) was recorded automatically by a PC.

2.3 Catalytic performance

Catalyst Evaluation experiment. FTs reaction was performed in a fixed bed tubular reactor (i.d. = 12 mm) at 2.0 MPa, 1000 h^{-1} and a H_2/CO ratio of 2.0. About 2 ml fresh catalyst (60~80 mesh) was mixed with the same volume silica sand to minimize the temperature gradient and reduced in a flow of hydrogen (GHSV=1000 h^{-1}) at 400 ^{o}C for 6 h and then cooled down to ambient temperature before switching to premixed syngas. Data were taken at steady state after 48 h on-stream. The gas effluents were analyzed on-line by using Carbosieve-packed column with TCD. The gas hydrocarbons were analyzed on-line using Porapack-Q column with flame ionization detector (FID). Liquid products and wax were collected in a cold trap and a hot trap, respectively, and were off-line analyzed on a GC-2010 chromatograph, which was equipped with a 35 m OV-101 capillary column. 5% N_2 was added into syngas as an internal standard. The carbon balance and mass balance were 100±5%.

The catalytic performance of catalyst was evaluated by CO conversion(X_{CO}) and C_5+ selectivity(S_{C5+}) with the following equations.

$$X_{CO}(\%) = \frac{\text{Moles of CO reacted}}{\text{Moles of CO supplied}} \times 100\% \quad (1)$$

$$S_{Cn}(\%) = \frac{\text{Moles of Cn formed}}{\text{Moles of Cn reacted}} \times 100\% \quad (2)$$

$$S_{5+}(\%) = 1 - \sum_{i=1}^{n=4} \text{Scn} \quad (3)$$

3 Results and discussion

3.1 Texture of the samples

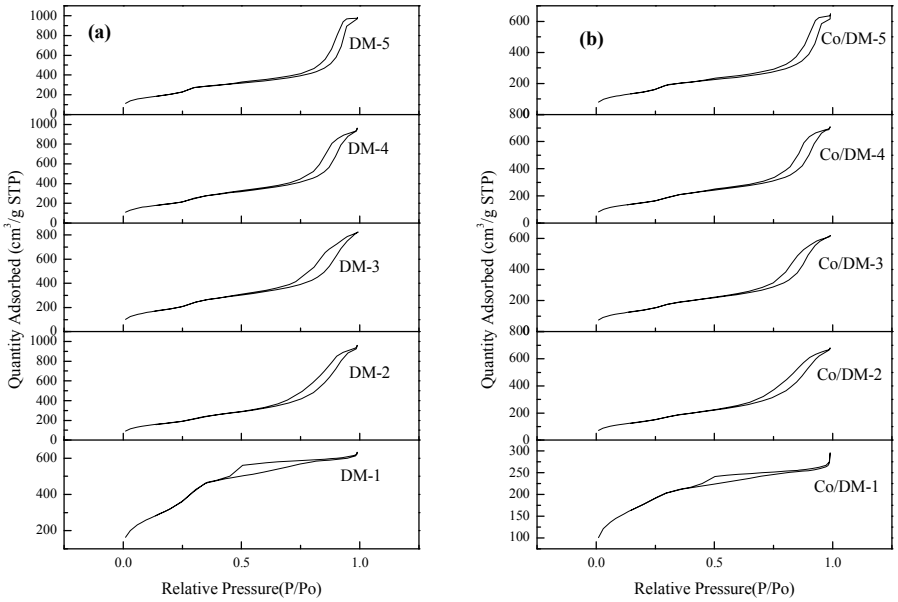

Fig.1 N_2 physisorption curves of the supports (a) and corresponding catalysts (b)

The isotherms of nitrogen adsorption and desorption, and the corresponding pore size distribution curves calculated using BJH method[15] of the supports and the corresponding catalysts are displayed in Fig.1(a), (b). The isotherms of bimodal supports and catalysts exhibited classical irreversible IV type adsorption isotherm with two separate and well expressed two distinct H_1 hysteresis loops at relative pressures P/Po of 0.2-0.4 and 0.8-1 according to the IUPAC classification. The first condensation step on the isotherm at 0.2-0.4 was similar to that for common MCM-41 materials with markedly higher saturation sorption capacity, though not very steep, which confirmed the mesoporous characteristics. The second condensation steps of the bimodal mesoporous catalyst on the isotherm at P/Po > 0.8 were steeper than the first ones and the hysteresis loops were wider. This indicated the presence of a significant amount of secondary mesoporous pore structure[16].

The BET surface area, total pore volume and average pore diameter of the supports and corresponding catalysts are presented in Table1. As shown in Table1, the bimodal catalysts all displayed large specific surface area due to the smaller pores of about 2.4 nm produced during the self-assembly process. Compared with the respective supports, the cobalt loaded catalysts showed lower BET surface area, pore volume and smaller average pore size, but the change of pore size distribution was not obvious. DM-1 support and Co/DM-1 catalyst showed the highest BET

surface area, due to their smaller pore size than that of others. Table 1 also showed that after loading with cobalt species, the BET surface areas were significantly reduced. This influence was especially obvious to the catalysts Co/DM-1, which might be due to the blocking of the pores by cobalt or a collapse of the pore structure[17]. And it clearly showed a very narrow bimodal mesoporous distribution. However, the data suggested that the pore structure of catalyst was not completely destroyed and still present bimodal mesoporous structure, just like that of supports.

Table 1 Physico-chemical properties of the samples

Samples	Surface area (m^2/g)	Pore Volume (cm^3/g)	Average pore diameter (nm)	Pore size (nm)		Crystalline size [a] (nm)	Dispersity[b] %	Loss of BET(%)	Reducibility[c] （%）
DM-1	1187.9	0.98	3.29	2.52	3.73				
DM-2	649.2	1.49	9.15	2.47	9.56				
DM-3	692.1	1.32	6.49	2.41	11.31				
DM-4	716.8	1.49	8.32	2.44	13.18				
DM-5	744.1	1.52	8.18	2.38	18.37				
Co/DM-1	643.0	0.46	2.85	2.37	8.77	14.2	6.8	54.12	19
Co/DM-2	507.4	1.05	8.31	2.4	11.21	22.3	4.3	78.15	47
Co/DM-3	483.2	0.96	7.58	2.39	14.38	12.0	8.0	69.81	38
Co/DM-4	545.3	1.09	8.05	2.46	18.43	19.7	4.9	76.07	43
Co/DM-5	527.1	1.01	7.63	2.45	22.52	30.7	3.1	70.83	49

a,Obtained by Scherrer equation $d = k\lambda/\cos\theta$; b,Calculated by: D% = 96/d(nm); c,Calculated by TPR from 60 to 400 °C

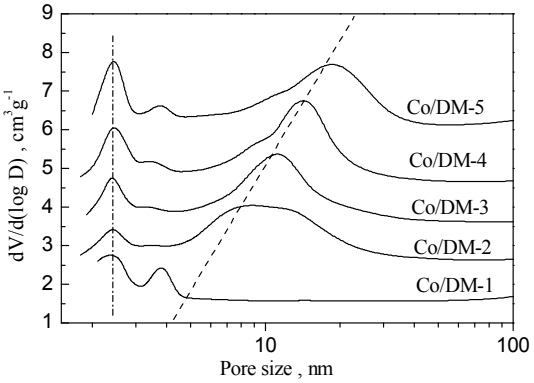

Fig.2 Curves of pore size distribution of the samples

Fig.2 displays the pore size distribution of bimodal catalysts. It could be clearly observed the obviously different bimodal mesporous distribution. As shown in Fig.2, the first pore was almost indentical (about 2.5 nm), which was similar to that of common MCM-41 materials. However, the second pores were different obviously, corresponding to 8 nm for Co/DM-1, 11 nm for Co/DM-2, 14 nm for Co/DM-3, 18 nm for Co/DM-4 and 22 nm for Co/DM-5, respectively.

3.2 Phase structure of the samples

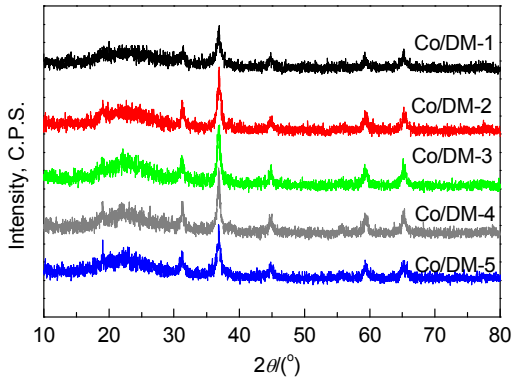

Fig.3 XRD patterns of the Catalysts

The X-ray powder diffraction patterns of the bimodal-pore catalysts are presented in Fig.3, and the average crystallite diameters of Co_3O_4, calculated by the Scherrer equation[18] ($2\theta = 36.9^o$), are listed in Table 1. For all the catalysts, different diffraction peaks at 2θ of 31.4^o, 36.9^o, 44.8^o, 59.4^o, 65.2^o were corresponding to the spinel Co_3O_4 crystalline phase (JCPDS no. 48-1719)[19, 20]. With the variation of pore size, the size of Co_3O_4 crystallite changed from 12.0 to 30.7 nm for the bimodal porous catalysts. Clearly, Co/DM-3 had the smallest Co_3O_4 crystallite size in these samples, whereas the Co-DM-5 had the biggest one, this result was not consistent with the literatures[5], which showed that the crystallite diameter increased with the increase of pore size.

3.3 SEM of the samples

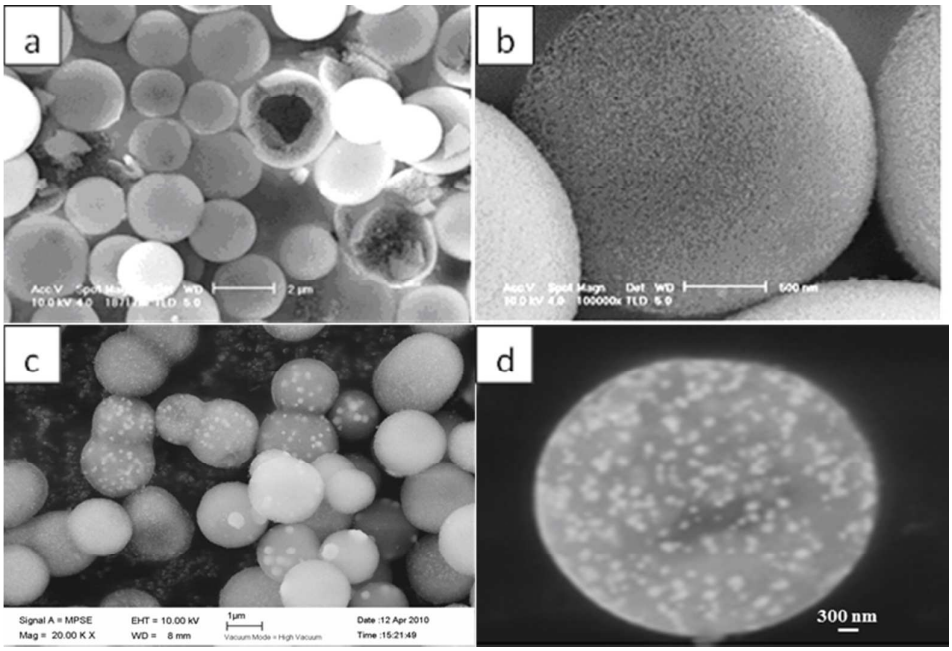

Fig.4 SEM image of support DM-3 (a,b) and corresponding catalyst Co/DM-3 (c,d)

Fig.4 showed the SEM micrographs of the catalysts with bimodal mesoporous distribution. SEM investigation provides a direct observation of the morphology and distribution of cobalt particles in the support. The morphology of bimodal mesoporous support was of spheres with a diameter about 2 μm. The broken section showed the hollow structure of support, and the thickness of shell was about 500 nm. A closer look at the surface of support from SEM revealed it was composed by rough and mesoporous SiO_2 materials. Fig.4 c and d displayed the presence of a considerable number of small cobalt clusters（about 100 nm） and well homogeneous cobalt distribution.

3.4 Transmission electron microscopy

To get a better understanding of the morphology and distribution of active species, TEM analysis was conducted. As shown in Fig.5, the sphere support surface comprised loose mesoporous materials, showing a rough surface. Combined with the pore size distribution curves, TEM image of the catalysts presented two kind of pore structures, one was one-dimensional straight pore channel structure, showing a hexagonal structure; the other a relatively larger pore was accumulational pore with a disordered and worm-like structure. The TEM results showed that cobalt species mainly dispersed in the two pore structure.

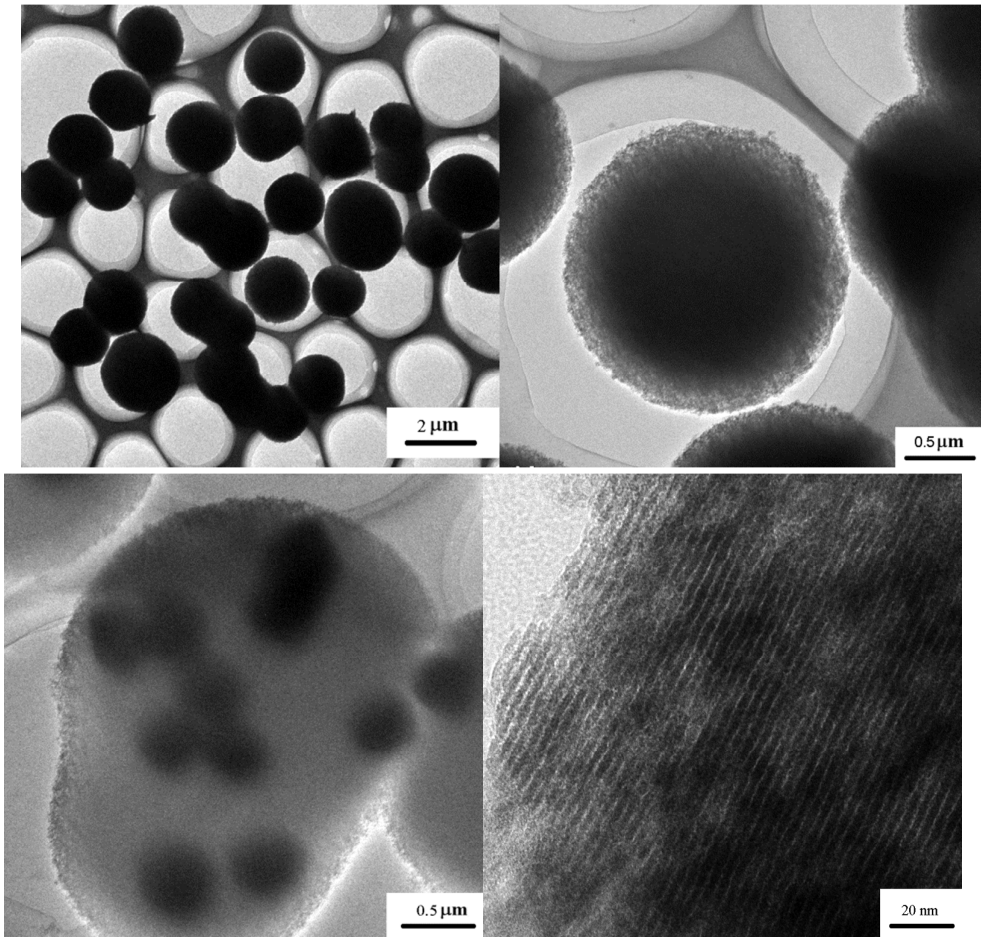

Fig.5 TEM morphology image of Co/DM-2

3.5 Reduction behavior of the samples

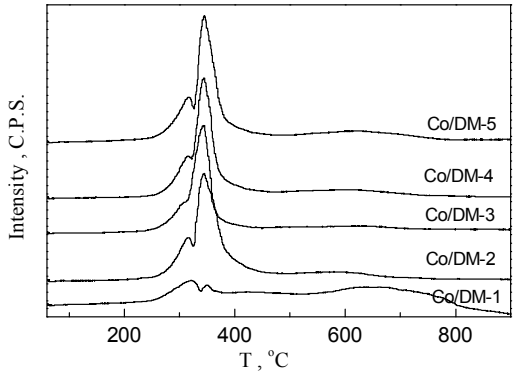

Fig.6 H_2-TPR curves of the catalysts

The influence of bimodal pore size on the reduction behavior of the catalysts was studied by TPR. Fig.6 shows the TPR profiles of the bimodal catalysts. The occurrence of multiple reduction peaks indicated the presence of a number of reducible cobalt species. Obviously, all the TPR profiles showed two major regions: a lower temperature region located between 250 and 400 ^{o}C and a higher temperature region located between 550 and 800 ^{o}C. The TPR peaks in the temperature range of 250–400 ^{o}C could be assigned to the two step reduction of Co_3O_4 ($Co_3O_4 \rightarrow CoO \rightarrow Co^0$)[14, 21, 22]. The broad peak between 550 and 800 ^{o}C was related to the reduction of cobalt oxide species (Co^{2}+ and Co^{3}+), which interacted with the support and were difficult to be reduced[23, 24]. It could be seen that the low temperature peak changed slightly except for the Co/DM-1 catalyst. As Table 1 shown, the catalyst Co/DM-1 with the smallest second pore size and the smallest surface area loss showed the lowest degree of reduction, while the catalysts of Co/DM-2, Co/DM-4 and Co/DM-5 showed similar reducibility. This was consistent with what had previously reported that small particles in narrow pores were more difficult to be reduced than larger particles in wide pores[8]. For all of the bimodal catalysts, the peak at around 217 ^{o}C did not appear, which indicated the interaction of cobalt salt and support became weaker and all of the cobalt nitrate precursor decomposed completely after calcination. Clearly, that was obviously different with mono-modal catalyst that had been reported previously [25].

3.6 Fischer-Tropsch synthesis reaction behavior

The catalytic performances of Co-based catalysts with different bimodal pore size distributions are listed in Table 2. It should be noted that all of the catalytic data were collected after 48 h on stream, when a steady state for the formation of the product was obtained.

3.6.1 Activity of bimodal catalysts

The activity and selectivity results for F-T synthesis are listed in Table 2. Many studies of F-T synthesis had suggested that the pore size of support could significantly affect the F-T reaction rate and hydrocarbon selectivity[26-28] . As shown in Fig.7, all bimodal porous catalysts present that with the increase of reaction temperature, the activity increased. This was because with the increase of reaction temperature, the energy of reactant enhanced, accordingly, the probability of collision of active sites increased, which promoted the conduct of reaction. Also, it could be seen from Table 2, under the same reaction temperature, that the Co/DM-5 catalyst with wider bimodal pore distribution showed the highest CO conversion, about 79%, which was better than that of Co/DM-1 and Co/DM-2. The low

activity on Co/DM-1 catalyst could be related to the small cobalt crystallite size, which resulted in the strong interaction between active species and support and low reducibility of cobalt species. In addition, as the BET result shown, the narrow bimodal pore distribution also caused more collapse and blocking pore, which hindered reactants to approach the active sites, leading to lower CO conversion rates. Meanwhile, the Co/DM-5 catalyst showed the high catalytic activity, maybe due to its larger particle size and high reducibility. From the obtained results, we could deduce that CO conversion increased with the increase of bimodal pore size. That was to say, the bimodal catalysts with larger second pore showed higher activity than that with smaller one, under the condition of the same first pore size, which was like the single pore structure catalysts[15, 29].

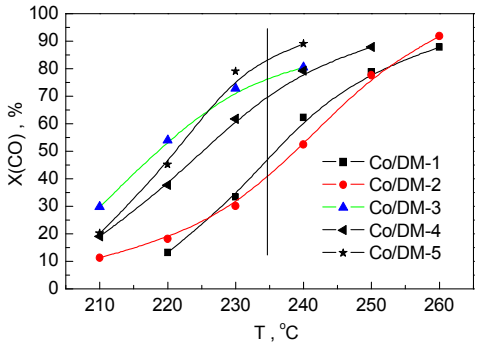

Fig.7 Relationship between reaction temperature and activity

Table 2 Activity and selectivity of different bimodal porous catalysts for Fischer-Tropsch synthesis

Cat	*X(CO) /(%)*	Distribution of hydrocarbons / (%)						
		C_1	C_{2-4}	C_{5-11}	C_{12-18}	C_{5-18}	C_5+	C_{19}+
Co/DM-1	33.5	6.8	5.0	24.1	37.6	61.7	88.2	26.5
Co/DM-2	30.2	6.9	7.0	23.1	32.5	55.6	86.1	30.5
Co/DM-3	72.8	7.9	1.6	24.7	28.1	52.8	90.5	37.7
Co/DM-4	61.7	15.7	12.4	27.6	31.0	58.6	71.9	13.3
Co/DM-5	79.0	9.9	10.5	31.1	34.4	65.5	79.6	14.1

Reaction conditions: $n(H_2)/n(CO) = 2.0$, GHSV = 1000 h^{-1}, p = 2.0 MPa, T=230 °C

3.6.2 Product selectivity of bimodal catalysts

Generally, support effects on the product selectivity were more complicated than on the activity. The pore size was one of the key factors for the catalyst performance, and it affected the size of cobalt oxide particles, the mass transfer of reactants and products, the re-adsorption of α-alkene, and the chemisorption ratio of H_2 and CO on the surface active sites. Moreover, the bimodal mesoporous

catalysts were favor to the re-adsorption of α olefin[5, 30], chain increasement and production distribution, which increased the selectivity of middle distillate.

Table 2 displays the activity and selectivity of different bimodal porous catalysts were markedly depending on their pore structure. The bimodal mesoporous catalysts showed a low methane selectivity, but when the pore size increased to an extent, the methane selectivity decreased again. This indicated that the catalysts with smaller pore showed the lower methane selectivity.

Considering product distributions for the five bimodal porous catalysts, we focused on the lager pores since these catalysts had similar smaller pores of around 2.4 nm in average pore size. F-T synthesis reaction was a complex reaction; and there were many factors that affected the product selectivity. It could be seen from Table 2, under the same reaction temperature, the C_5+ selectivity of all catalysts presented volcano curve, and the Co/DM-3 catalyst with an appropriate pore size of 2.5 and 14 nm showed the highest C_5+ selectivity. This result was likely due to the suitable bimodal mesoporous structure, which enhanced the facile dissociation of CO and diminished the diffusion resistance, and favored chain-growing process of intermediates to further generate heavy hydrocarbons[30]. Moreover, it could be clearly seen from Fig.8, the heavy hydrocarbon selectivity of catalysts with large second pore size was lower than that with narrow second pore. This phenomenon might be ascribe to the cracking of heavy hydrocarbon, and it also showed large pore channel favored the desorption and diffusion of production, and the mass transportation was easy to conduct, which was consistent with the report[7]. In addition, the catalyst with larger second pore size showed higher middle distillate selectivity, especially Co/DM-5 catalyst showed higher $C_{5\text{-}18}$ selectivity, about 65%. Based on the obtained characterization and catalytic performance result, the high $C_{5\text{-}18}$ selectivity of Co/DM-5 catalyst was likely due to its larger mesoporous size, which could favor the desorption and diffusion of reactants and production.

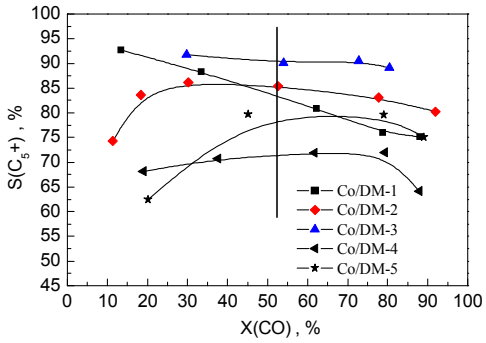

Fig.8 Relationship of C_5+ selectivity and activity

4 Conclusions

Characterization and catalytic performance results showed that the support with bimodal structure influenced strongly the structure, the reducibility and the F-T catalytic performance of bimodal mesoporous cobalt catalysts. Catalytic results showed the bimodal catalysts with larger second pore showed higher activity, methane selectivity and lower heavy hydrocarbon selectivity than that with smaller ones, under condition of the same first pore size. Especially Co/DM-5 catalyst with a bimodal 2.5 and 22 nm pore size distribution presented higher $C_{5\text{-}18}$ selectivity, about 65%.

Acknowledgements

This work was supported by Shell-SARI STRATEGIC COOPERATION AGREEMENT (PT31043) and the Natural Science Foundation of China (No. 21203232 and 21273265).

References

1. C. Ngamcharussrivichai, X. H. Liu, X. H. Li, T. Vitidsant and K. Fujimoto, *Fuel*, 2007, 86, 50-59.
2. P. Munnik, P. E. de Jongh and K. P. de Jong, *J Am Chem Soc*, 2014, 136, 7333-7340.
3. M. Sarkari, F. Fazlollahi, H. Ajamein, H. Atashi, W. C. Hecker and L. L. Baxter, *Fuel Processing Technology*, 2014, 127, 163-170.
4. B. L. Xu, Y. N. Fan, Y. Zhang and N. Tsubaki, *Aiche J*, 2005, 51, 2068-2076.
5. Y. Zhang, M. Koike, R. Q. Yang, S. Hinchiranan, T. Vitidsant and N. Tsubaki, *Appl Catal a-Gen*, 2005, 292, 252-258.
6. M. Shinoda, Y. Zhang, Y. Yoneyama, K. Hasegawa and N. Tsubaki, *Fuel Processing Technology*, 2004, 86, 73-85.
7. S. J. Park, J. W. Bae, J. H. Oh, K. V. R. Chary, P. S. S. Prasad, K. W. Jun and Y. W. Rhee, *J Mol Catal a-Chem*, 2009, 298, 81-87.
8. C. l. Guo, Y. Y. Wu and J. S. Zhan, *Reaction Kinetics, Mechanisms and Catalysis*, 2013, 109, 497-508.

9. Q. H. Zhang, J. C. Kang and Y. Wang, *Chemcatchem*, 2010, 2, 1030-1058.
10. Y. Zhang, M. Shinoda and N. Tsubaki, *Catal Today*, 2004, 93-95, 55-63.
11. X. Y. Li, M. H. Sun, J. C. Rooke, L. H. Chen and B. L. Su, *Chinese Journal of Catalysis*, 2013, 34, 22-47.
12. J. G. Wang, D. B. Li, B. Hou, L. T. Jia, J. G. Chen and Y. H. Sun, *Catalysis Letters*, 2010, 140, 127-133.
13. G. Schulz-Ekloff, J. Rathousky and A. Zukal, *Int J Inorg Mater*, 1999, 1, 97-102.
14. H. l. Li, S. G. Wang, F. X. Ling and J. L. Li, *Journal of Molecular Catalysis A: Chemical*, 2006, 244, 33~40.
15. A. Y. Khodakov, A. Griboval-Constant, R. Bechara and V. L. Zholobenko, *Journal of Catalysis*, 2002, 206, 230-241.
16. A. Barrera, K. Muramatsu, T. Viveros, S. Gomez, J. A. Montoya, P. del Angel, G. Perez and J. Campa-Molina, *Appl Clay Sci*, 2009, 42, 415-421.
17. W. S. Yang, D. Y. Fang, H. W. Xiang, Y. W. Li and J. S. Liu, *Chinese Journal of Catalysis*, 2005, 26, 329-334.
18. O. A. Bulavchenko, S. V. Cherepanova and S. V. Tsybulya, *Zeitschrift für Kristallographie Supplements*, 2009, 2009, 329-334.
19. A. Y. Khodakov, R. Bechara and A. Griboval-Constant, *Appl Catal a-Gen*, 2003, 254, 273-288.
20. E. Lira, C. M. Lopez, F. Oropeza, M. Bartolini, J. Alvarez, M. Goldwasser, F. L. Linares, J. F. Lamonier and M. J. P. Zurita, *J Mol Catal a-Chem*, 2008, 281, 146-153.
21. H. L. Li, J. l. Li, H. K. Ni and D. C. Song, *Catalysis Letters*, 2006, 110, 71-76.
22. A. Y. Khodakov, W. Chu and P. Fongarland, *Chem Rev*, 2007, 107, 1692-1744.
23. Y. Zhang, Y. Yoneyama, K. Fujimoto and N. Tsubaki, *Topics in Catalysis*, 2003, 26, 129-137.
24. B. Jongsomjit and J. G. Goodwin, *Catal Today*, 2002, 77, 191-204.
25. D. C. Song and J. L. Li, *Journal of Molecular Catalysis A: Chemical*, 2006, 247, 206~212.
26. C. M. A. Parlett, K. Wilson and A. F. Lee, *Chemical Society Reviews*, 2013, DOI: 10.1039/c2cs35378d.
27. E. van Steen and M. Claeys, *Chem Eng Technol*, 2008, 31, 655-666.
28. W. P. Ma, G. Jacobs, D. E. Sparks, M. K. Gnanamani, V. R. R. Pendyala, C. H. Yen, J. L. S. Klettlinger, T. M. Tomsik and B. H. Davis, *Fuel*, 2011, 90, 756-765.
29. O. Borg, N. Hammer, S. Eri, O. A. Lindvag, R. Myrstad, E. A. Blekkan, M. Ronning, E. Rytter and A. Holmen, *Catal Today*, 2009, 142, 70-77.
30. H. F. Xiong, Y. H. Zhang, S. G. Wang and J. L. Li, *Catalysis Communications*, 2005, 6, 512~516.